Molecular Cancer

RESEARCH

Open Access

Intercellular TIMP-1-CD63 signaling directs the evolution of immune escape and metastasis in KRAS-mutated pancreatic cancer cells

Chu-An Wang[1,2†], Ya-Chin Hou[3,9†], Yi-Kai Hong[4], Yu-Jing Tai[1], Chieh Shen[2], Pei-Chi Hou[5], Jhao-Lin Fu[1], Cheng-Lin Wu[6], Siao Muk Cheng[7], Daw-Yang Hwang[7], Yung-Yeh Su[7,8,11,12], Yan-Shen Shan[3,9*] and Shaw-Jenq Tsai[2,10*]

Abstract

Background and aims Oncogenic KRAS mutations are present in approximately 90% of pancreatic ductal adenocarcinoma (PDAC). However, Kras mutation alone is insufficient to transform precancerous cells into metastatic PDAC. This study investigates how KRAS-mutated epithelial cells acquire the capacity to escape senescence or even immune clearance, thereby progressing to advanced PDAC.

Methods Single-cell RNA sequencing and analysis of primary PDAC tumors were conducted. Genetically engineered pancreas-specific Kras-mutated, dual specificity phosphatase-2 (Dusp2) knockout mouse models were established. Human and mouse primary pancreatic cancer cell lines were used for in vitro assessment of cancer characteristics. Tumor progression was studied via pancreas orthotopic and portal vein injection in the immune-competent mice. Clinical relevance was validated by digital spatial transcriptomic analysis of PDAC tumors.

Results Kras mutation induces the formation of pancreatic intraepithelial neoplasia (PanIN), these lesions also exhibit significant apoptotic signals. Single-cell RNA sequencing identified a subset of $ERK^{active}DUSP2^{low}$ cells continuing to expand from early to advanced stage PDAC. In vitro and in vivo studies reveal that early infiltrating macrophage-derived tissue inhibitor of metallopeptidase 1 (TIMP-1) is the key factor in maintaining the $ERK^{active}DUSP2^{low}$ cell population in a CD63-dependent manner. The $ERK^{active}DUSP2^{low}$ cancer cells further exacerbate macrophage-mediated cancer malignancy, including loss of epithelial trait, increased lymphangiogenesis, and immune escape. Digital spatial profiling analysis of PDAC samples demonstrates the colocalization of $TIMP\text{-}1^{high}$ macrophages and $CD63^{high}$ cancer cells. The presence of $TIMP\text{-}1^{high}$ macrophages and $CD63^{high}$ epithelial cells correlates with poor prognosis in PDAC.

Conclusions Our study reveals the vicious cycle between early infiltrating macrophages and pancreatic cancer cells, providing a mechanistic insight into the dynamic regulation directing pancreatic cancer progression.

†Chu-An Wang and Ya-Chin Hou contributed equally to this work.

*Correspondence:
Yan-Shen Shan
ysshan@mail.ncku.edu.tw; ysshan2006@gmail.com
Shaw-Jenq Tsai
seantsai@ccu.edu.tw

Full list of author information is available at the end of the article

Introduction

Oncogenic KRAS mutation is considered the driver mutation, which is found in about 90% of pancreatic ductal adenocarcinoma (PDAC) [1] and also in about 30% of pancreatic intraepithelial neoplasia (PanIN) [2]. In the transgenic mouse models, Kras activation could initiate the formation of PanIN [3], while further progression to PDAC requires a prolonged latency which can be accelerated by the inactivation of tumor suppressors such as Ink4a/Arf or P53 [4, 5]. Mitogen-activated protein kinase (MAPK)/extracellular signal-regulated kinases (ERK) signaling is considered a downstream effector of RAS and ERK inhibition has been shown to exhibit synergistic effects in combination strategies [6]. Interestingly, it was found that persistent activation of ERK induced rapid formation of PDAC in Kras mutated pancreas while Kras activating mutation was insufficient to induce prolonged ERK signaling [7]. These results indicated that higher level of ERK activation during PDAC progression is regulated by an unidentified mechanism. Given the crucial role of ERK activation in supporting the progression of Kras-mutated pancreatic cancer, it warrants further investigation.

One of the unique characteristics of PDAC is that the proliferation of PDAC cells is not profound, but metastasis occurs at very early stages. For PDAC, tumor cells compose only 10% of the tumor mass and the rest are stromal components. In addition to the extracellular matrix, the stromal compartment comprises different cells, including endothelial cells, fibroblasts, stellate cells, immune cells, and neurons. Bidirectional interaction between cells in the tumor microenvironment has been demonstrated to affect tumor growth, metastasis, or drug response [8]. However, what kind of interactions drive the Kras-mutated precancerous cells slowly transform into metastatic PDAC remains largely uncharacterized. Infiltrating immune cells, including lymphoid and myeloid lineages, are one of the predominant populations within the tumor microenvironment [9], which is known to be extensively involved in tumor progression such as chemoresistance, angiogenesis, stroma remodeling, metastasis and immune suppression [10–14]. In the precancerous lesion of the pancreas, macrophages are recruited by ICAM-1 and facilitate Kras mutation-mediated transformation [15], suggesting the importance of a cooperative mechanism between oncogenic mutation and inflammation in cancer development. The observation of early infiltrating macrophages in PanIN further suggests their role in the initiation stage of tumor development [16, 17]. As the tumor continues to develop, the constitutive recruitment of macrophages contributes to cancer progression in a CXCL8-dependent manner or via the PGE_2–IL-1β axis [18, 19]. Systematic depletion of macrophages in a transgenic mouse model of pancreatic cancer showed markedly reduced metastasis in the liver and lung without a significant impact on primary tumors [20], implying the role of macrophages in promoting specifically the metastatic ability of pancreatic cancer. However, as cell interaction in the tumor microenvironment is dynamic and diverse subsets of macrophages have been discovered, the mutual regulation between macrophages and tumor cells remains to be fully understood.

In this study, we investigated the impact of tumor microenvironment in amplifying ERK activity in pancreatic cancer cells. We identified that unpolarized macrophages, which mimic early infiltration population, not only quickly induced ERK1/2 phosphorylation but also sustained its activity via suppression of its suppressor, dual specificity phosphatase 2 (DUSP2). Inhibition of DUSP2 in PDAC cells recapitulated the effects of macrophages in regulating metastatic abilities. Once the ERK-DUSP2 axis was initiated, subsequent amplification via macrophage-tumor cell interaction further leads to the creation of an immune suppressive microenvironment. Our study reveals the molecular mechanism of how early infiltrating macrophages cultivate metastatic tumor cells and create an immune suppressive environment, establishing the vicious cycle and sustaining tumor progression.

Material and method

Cell culture and conditioned medium preparation

Pancreatic cancer cell line PANC-1, AsPC-1, MIA PaCa-2 (RRID: CVCL_0428), and monocyte cell line (U937, RRID: CVCL_0007) were maintained in RPMI 1640 media containing 10% fetal bovine serum (FBS), glutamine, and sodium pyruvate. Human pancreatic stellate cell line was purchased from ScienceCell (#3830) and maintain according to the manufacturer's protocol. To differentiate U937 cells into macrophages, 4×10^6 U937 cells were treated with 0.5 μM phorbol myristate acetate (PMA) and cultured in 10 ml complete medium in 10 cm petri dish for two days. After then, cells were replaced with 10 ml fresh medium for another 24 h. Macrophage conditioned medium (MCM) was collected and first centrifugation by 500 g 10 min to remove cell debris and then filtered by 0.22 μm filter. MCM was used to treat PDAC cells or stored at -20 °C. 6-well inserts with pore size of 0.4 μm was used for co-culture assay (MCHT06H48, Millipore). DUSP2 stable knockdown PANC-1 cells were established as previous described [21]. CD63 stable knockdown was achieved by shRNA clones from GeneCopoeia (HSH063212). To establish MCM-selected PANC-1 cells, 50% MCM with 50% fresh medium was added to PANC-1 cells every two days. When reach confluency, cells were subcultured and replated in the medium as described above. MCM selection was carried out for a month. KPPC cell line was

isolated from a pancreatic tumor developed in KPPC transgenic mouse model (KrasLSL.^{G12D};Trp53$^{R172H/R172H}$; Pdx1-Cre, oncogenic Kras mutation and homozygous mutation of the P53 allele). Cell lines were cultured in a humidified atmosphere of 5% CO_2 and 95% air incubator at 37 °C. Cell lines used in the study have been authenticated and tested as mycoplasma free.

Monocyte isolation and co-culture assay

Heparinized blood was collected from healthy donors under informed consent. Peripheral blood mononuclear cells (PBMCs) were isolated using Ficoll-Paque density gradient centrifugation at 400× g for 20 min. PBMCs from buffy coat layer were collected and washed three times with 1× PBS. Monocytes were stained with anti-CD14-conjugated FITC antibody (Genetex 75931) and then sorted using a BD FACSCanto II (Becton Dickinson, New York, USA). $CD14^+$ monocytes were used only if purity was >90% by FACS analysis. $CD14^+$ monocytes or U937 cells (3×10^5/well) were seeded in 6-well plates. An equal number of human pancreatic cancer cells were seeded in the Transwell inserts (polycarbonate membranes with 4 μm pores) and co-cultured with monocytes for 3 days.

In vitro cell function assays

To measure cell migration ability, 1×10^5 MIA PaCa-2 cells were suspended in 200 μl serum-free RPMI medium and then added in 24-well Transwell inserts with pore size of 8.0 μm (PIEP12R48, Millipore). 500 μl 10% FBS RPMI medium were added to the lower chamber. The transwell inserts were incubated for 16 h in 37 °C. Inserts were washed by PBS and fixed with 95% ethanol for 15 min. Cells were stained with 0.02% crystal violet and washed by H_2O until background was clear. Cell numbers were counted by ImageJ cell counter (RRID: SCR_003070). To measure cell viability in suspension, 2×10^5 pancreatic cancer cells were resuspended in ultra-low plate (Corning 3471) for 24 h. Cells were stained for Annexin V (BD 556547) followed by the manufacturer's protocol and apoptotic cells were analyzed by flow cytometry.

RT-qPCR and Western blot analysis

Total RNA was subjected to RT-qPCR as previously described. Transcripts were quantified by Applied Biosystem StepOne. SYBR green assay primers sequence as follows: *DUSP2* F: GCCCACTGCCGTGTACTTC, *DUSP2* R: TGGTTTTGTCCCCTGTTGG; *CDH1* F: ACGCATT GCCACATACACTC, *CDH1* R: ATTCGGGCTTGTTG TCATTC; *VEGFC* F: AATAGTGAGGGGCTGCAGTG, *VEGFC* R: TTGGGGCCTTGAGAGAGAG. *GAPDH* F: AATCCCATCACCATCTTCCA, *GAPDH* R: TGGACT CCACGACGTACTCA; *CD274* F: AAATGGAACCTGG CGAAAGC, *CD274* R: GATGAGCCCCTCAGGCATTT. Relative expression was normalized to the expression of *CYCLOPHILIN B* in the cells (F: CGTCTTCTTCCTGCT GCTG, R: CATCTTCATCTCCAATTCGTAGG). Whole cell lysates were collected by RIPA buffer and subjected to Western blotting as described previously [22]. Antibodies against Phospho-p44/42 MAPK (Cell Signaling Technology #4370, RRID: AB_2315112), p44/42 MAPK (Cell Signaling Technology #4696, RRID: AB_390780), DUSP2 (Santa Cruz sc32776, RRID: AB_2094883), E-cadherin (Cell Signaling Technology #3195, RRID: AB_2291471), VEGF-C (Genetex 113574, RRID: AB_10620764), PD-L1/CD274 (Proteintech: 66248-1-Ig, RRID: AB_2756526), GFP (Genetex, GTX113617, RRID: AB_1950371), tissue inhibitor of metallopeptidase 1 (TIMP-1, R&D, AF970), CD63 (ABclonal, A19023), β-actin (Sigma A1978, RRID: AB_476692), GAPDH (Genetex, GTX100118, RRID: AB_1080976) were used for Western blotting.

Immunohistochemistry (IHC) staining

Tumors from animals were fixed in 4% paraformaldehyde, embedded in paraffin, and cut into 5-μm sections. Primary antibodies against Lyve-1 (Angiobio 11–034, RRID: AB_2813732), CD31 (abcam ab28364, RRID: AB_726362), macrophage marker (SANTA CRUZ BIOTECHNOLOGY sc-66204, RRID: AB_2184280), F4/80 (abcam ab6640, RRID: AB_1140040), E-cadherin (Cell Signaling Technology #3195, RRID: AB_2291471), Ck19 (abcam ab133496, RRID: AB_11155282) were used for immunohistochemistry staining.

Animal studies

Male SCID mice (6- to 8-weeks of age) were used for pancreas orthotopic injection using PANC-1 pancreatic cancer cell line. 1×10^6 cells PANC-1 and MCM-selected PANC-1 cells were suspended in 100 μl of RPMI medium and injected into the pancreas of mice. Tumor cells isolated from KPPC mice (Kras$^{LSL-G12D/+}$, Trp53 $^{LSL-R172H/\ R172H}$, Pdx1$^{Cre/+}$) were used for pancreas and portal vein injection. KPPC cells were suspended in RPMI medium and matrigel (1:1) and 10^5 cells in 50ul was injected directly into pancreas of male B6 mice. KPPC cells were suspended in RPMI medium and 2.5×10^4 cells in 10ul was injected directly into portal vein of mice. Animals were kept in conventional animal facilities and monitored daily. Experimental procedures of animal studies were approved by the Institutional Animal Care and Use committee at the National Chung Kung University.

Tissue collection, single-cell or bulk RNA sequencing, and digital spatial profiling (DSP)

Tumor specimens were obtained from PDAC patients undergoing surgical resection at the National Cheng

Kung University Hospital (NCKUH) under Institutional Review Board (IRB)-approved protocol (IRB number: NCKUH B-ER-110-420). For single-cell analyses, fresh tumor tissues from patients with stage II (early, T2N0M0, pancreatic head adenocarcinoma, well differentiated) or III PDAC (advanced, T3N2M0, pancreatic head adenocarcinoma, moderately-differentiated, marked perineural invasion) were dissociated using a tumor dissociation kit (Cat #130-095-929, Miltenyi Biotec, Bergisch Gladbach, Germany). A total 5303 and 3167 cells, respectively, were processed for analysis. Cell suspension was then centrifuged at 800 rpm for 5 min to collect cell pallet and incubated with Red Blood Cell lysis buffer to removed erythrocytes. Cell viability was stained by trypan blue staining (Invitrogen), and measured by TC20TM automated cell counted (Bio-Rad) to ensure cell viability was greater than 70%. Single-cell sequencing libraries were prepared according to the standard protocol of the 10× Genomics Single Cell 3 v2 Reagent Kit. Final libraries were sequenced on a Novaseq 6000 (Illumina, San Diego, CA, USA) at a depth of ~20,000 reads per cell. For bulk RNA sequencing, total RNA from frozen tumor tissues were isolated using TRIzol (Invitrogen) followed by final purification through the Qiagen RNeasy MinElute kit (Qiagen). Library construction was prepared by using NEBNext Ultra RNA Library Prep Kit, validated on Agilent 2100 Bio-analyzer and Real-Time PCR System and then sequenced using Illumina HiSeq platform. Formalin-fixed, paraffin-embedded PDAC samples for DSP was performed according to the standard protocol of GeoMx DSP RNA assay (Whole Transcriptome Atlas; NanoString). The DSP barcodes containing UV-photocleavable oligos comprising PanCK (a marker for epithelium cells), CD45 (a marker for immune cells), and SYTO13 (nuclei) to allow for the morphological outline of sections were used synchronously. The DSP instrument was applied for high-resolution scanning (×20 objective lens) and selecting the regions of interest (ROIs). The UV-cleaved oligos from each ROI were collected, followed by PCR amplification and then subjected to Illumina NovaSeq instrument for sequencing.

Statistical analysis

Statistical analyses were performed by GraphPad Prism 5.00 (RRID: SCR_002798). The results were presented as mean ± standard error of the mean. Two-tailed Student's *t*-test was employed for comparing two groups. One-Way ANOVA and Tukey posttest was used to compare differences in more than two groups. Error bars represent the standard error of the mean from at least three independent experiments. Asterisks denote significant difference from control group *, $P < 0.05$; **, $P < 0.01$; ***, $P < 0.001$.

Results

Sustained ERK activity may be the driving force of KRAS-mutated PDAC progression

The high prevalence of KRAS mutation found in PDAC suggests its tumor-promoting function in cancer development. However, by immunohistochemistry staining of control and Kras mutated pancreas ($Kras^{LSL-G12D/+}$, $Pdx1^{Cre/+}$, KC), we found that PanIN regions were also highly positive for senescence and apoptosis signals (Fig. 1A and B and supplementary Fig. 1). This observation explains why Kras mutation inefficiently drives the progression from PanIN to PDAC. To investigate the underlying mechanism responsible for Kras-mutated cells transforming to malignant PDAC, we re-analyzed single-cell RNA sequencing dataset of murine pancreatic cancer, which encompasses normal pancreas, PanIN ($Kras^{LSL-G12D/+}$, $Ink4a^{fl/fl}$, $Ptf1a^{Cre/+}$, KIC), and PDAC ($Kras^{LSL-G12D/+}$, $Trp53^{LSL-R172H/+}$, $Ptf1a^{Cre/+}$, KPC; $Kras^{LSL-G12D/+}$, $Trp53^{fl/fl}$, $Pdx1^{Cre/+}$, KPfC) [23]. As tumor stage advanced, the shift from acinar to ductal can be observed (Fig. 1C and supplementary Fig. 2A-B). The epithelial population (acinar and ductal cells) was further clustered into eight subgroups (Fig. 1D). The proportion of two subgroups (E1 and E2) shows an increase from normal to early and late stage of PDAC (Fig. 1E), implying those two populations are expanding as tumor progresses. Pseudotime analysis revealed that E2 is enriched in the more advanced tumor stage (Fig. 1F and supplementary Fig. 2C-D) and with the expression of Krt18 and Krt19. In contrast, cluster E1 still have high level of acinar gene expression (Amy1/Amy2a2). Gene ontology enrichment analysis was performed to investigate the properties of these two populations (Fig. 1G). In E1 group, cellular response to inflammation, ion, and stress was identified, suggesting this population is receiving external stimuli. E2 group, which is very low in normal pancreas but significantly increases in early KIC, has enriched pathways of epithelial proliferation, ERK signaling, and migration and cytoskeleton organization. Since ERK activation has been shown to promote progression of Kras-mutated PanIN to PDAC [7] and ERK activity persists from low to high-grade PDAC ($Kras^{LSL-G12D/+}$, $Trp53^{LSL-R172H/\ LSL-R172H}$, $Pdx1^{Cre/+}$, KPPC) (supplementary Fig. 3), we thus further investigated how a subset of Kras-mutated cells acquire enhanced ERK activity.

To investigate the involvement of ERK activity in the transition from early to advanced PDAC, we performed single-cell RNA sequencing using early and advanced pancreatic tumors. Pancreatic tumors were separated into 21 distinct populations, belonging to 7 major cell types (Fig. 2A and B, and supplementary Fig. 4A-B). The proportion of cell population shows an increase in fibroblast, macrophage, and epithelial cells while a decrease in T and B cell population as tumor progressed from

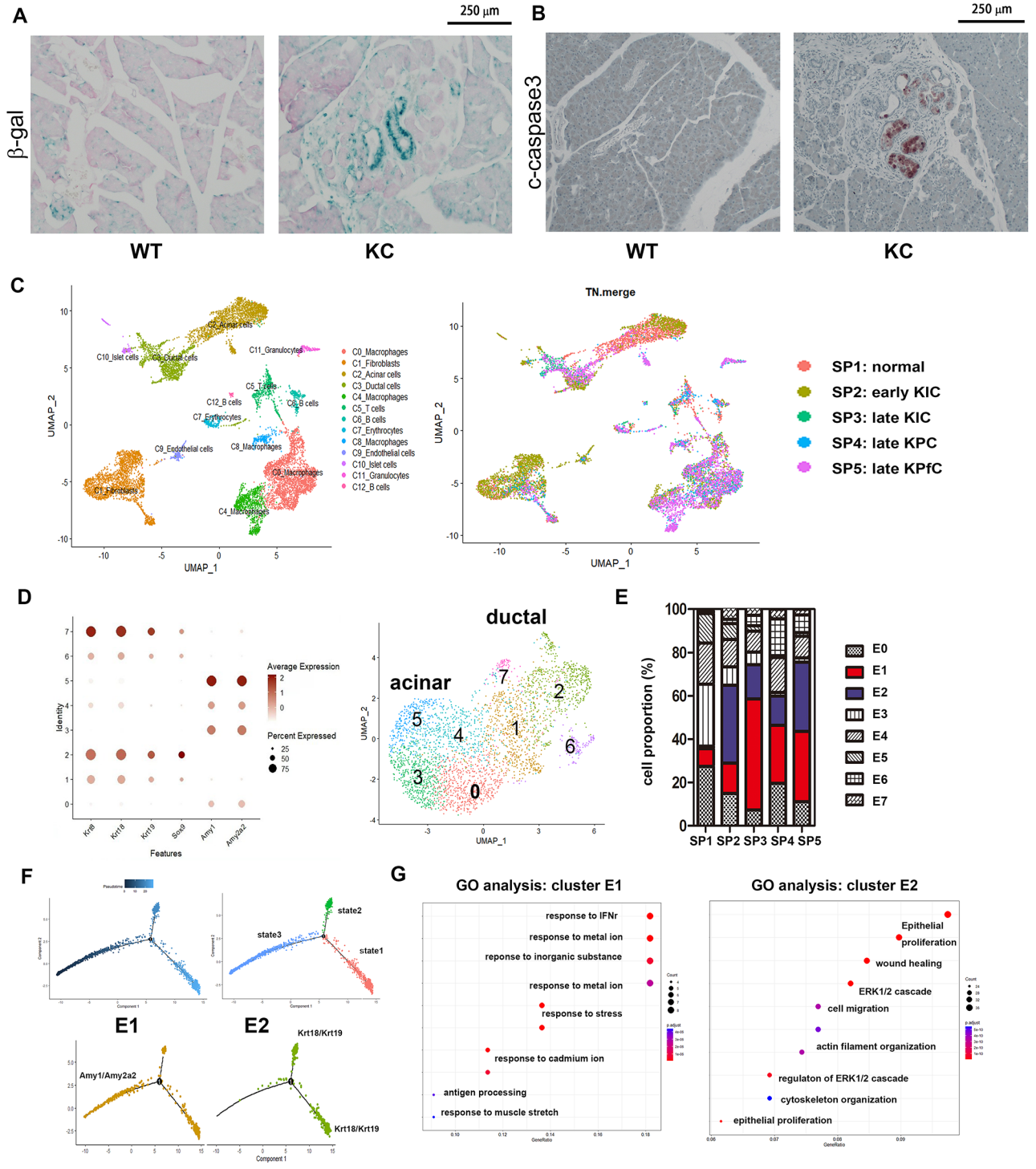

Fig. 1 A subset of Kras mutant epithelial cells expands as tumor progresses. (**A**) The expression of SA-β-Gal, which is present only in senescent cells, was detected in control and KC pancreas (abcam 65351). (**B**) Apoptosis in control and KC pancreas was detected by immunohistochemical staining for cleaved caspase-3. (**C**) Uniform Manifold Approximation and Projection (UMAP) plot of the normal, early/late lesion pancreas ($Kras^{LSL-G12D/+}$, $Ink4a^{fl/fl}$, $Ptf1a^{Cre/+}$, KIC), and PDAC ($Kras^{LSL-G12D/+}$, $Trp53^{LSL-R172H/+}$, $Ptf1a^{Cre/+}$, KPC; $Kras^{LSL-G12D/+}$, $Trp53^{fl/fl}$, $Pdx1^{Cre/+}$, KPfC) composing 13 distinct cell populations. (**D**) A dot plot shows the relative expression of selected genes in the epithelial cells (E0-E7) in mouse pancreatic tissue (left). UMAP plot of epithelial sub-clustering (right). (**E**) The proportion of each epithelial subsets in different stages of the pancreas. (**F**) Pseudotemporal ordering of epithelial cells (E0-E7) reveals a branched trajectory. The distribution of the 3 subpopulations is plotted on each of the branches (upper). The distribution of E1 and E2 subgroups on the pseudotime trajectory is shown (lower). (**G**) Gene ontology (GO) analysis of differentially expressed genes (DEGs) in E1 and E2

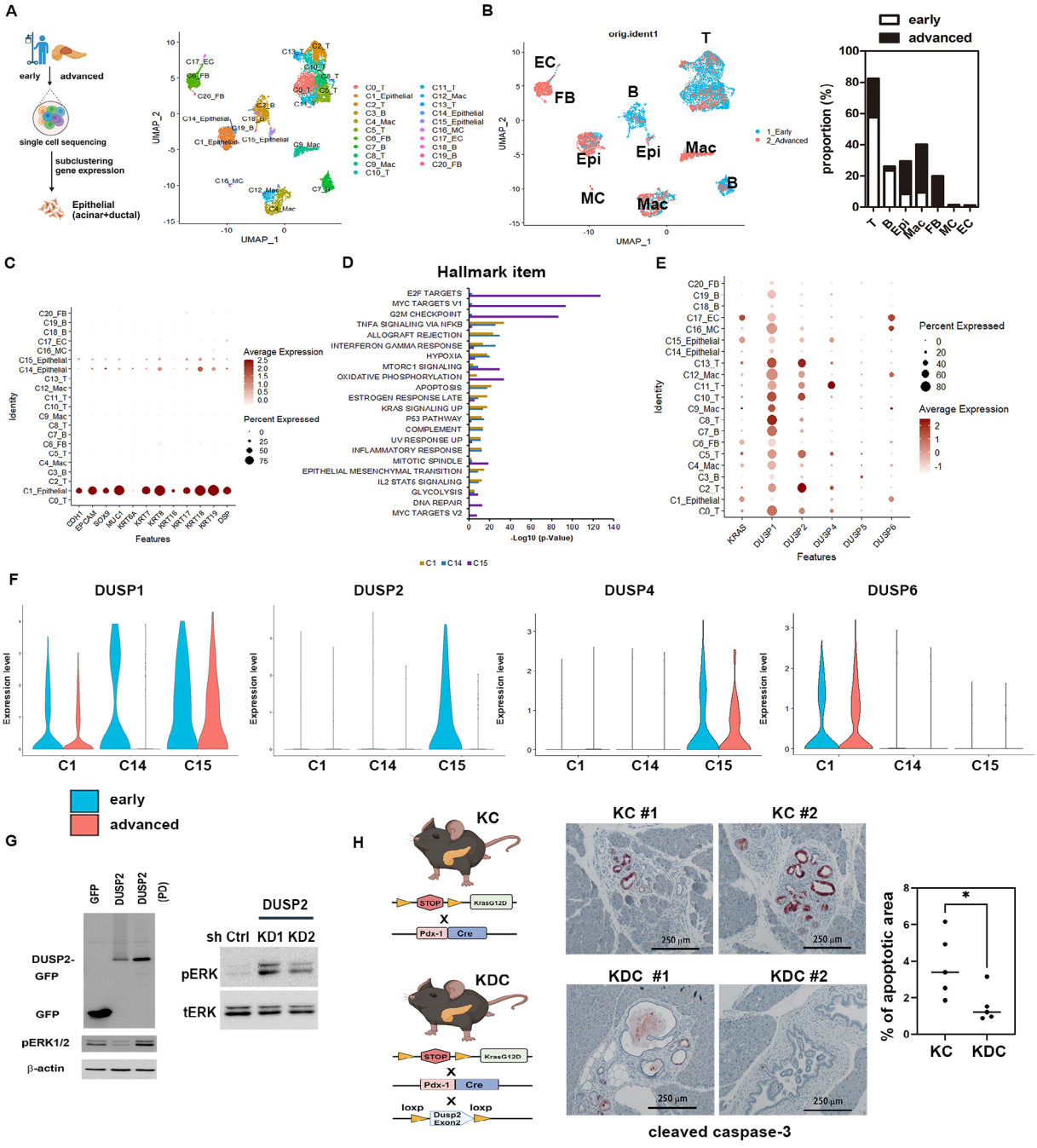

Fig. 2 Identify DUSPs expressing epithelial subsets and gene expression pathways. Schematic showing early and advanced PDAC were collected after surgery and processed for 10x scRNA-seq (left). UMAP plots of distinct populations are clustered by the average gene expression in early and advanced PDAC tumors. Each dot represents the transcriptome of a single cell, with color coding defining clusters of cells having similar transcriptional identities (right). (**B**) UMAP plots of distinct populations from early and advanced PDAC (left). Percentage frequency of cell populations in the scRNA-seq data between early and advanced PDAC are shown (right). (**C**) A dot-plot showing the relative expression of a subset of epithelial/ ductal marker genes (left). The color of each dot represents the average expression across the cluster, the size of each dot represents the percentage of cells in the cluster expressing the gene. (**D**) Hallmark pathway enrichment analysis of DEGs in three epithelial subsets (C1-Epi, C14-Epi, and C15-Epi) detected in a Stage II PDAC tumor. (**E**) A dot-plot showing the relative expression of KRAS, DUSP1, DUSP2, DUSP4, DUSP5, and DUSP6 in clusters of different cell type. (**F**) Violin plots showing the distribution of expression levels DUSP1, DUSP2, DUSP4, and DUSP6 in three subsets of epithelial populations in early and advanced tumors. (**G**) DUSP2 regulates ERK1/2 activity in PANC-1 cells. PANC-1 cells were transfected with GFP, DUSP2-GFP, and phosphatase dead DUSP2-GFP (PD) for 24 h. Western blotting was performed to determine pERK1/2. β-actin is the loading control. GFP was used for the detection of exogenous DUSP2 expression (left). Western blotting was performed to determine pERK1/2 and total EKR1/2 (tERK1/2) in control and DUSP2-KD PANC-1 cells (right). (**H**) Representative (left) and quantification (right) of immunohistochemical staining images show expression of cleaved caspase-3 in the lesion of KC ($Kras^{LSL-G12D/+}$, $Pdx1^{Cre/+}$) and KDC ($Kras^{LSL-G12D/+}$, $Dusp2^{fl/fl}$, $Pdx1^{Cre/+}$) transgenic mouse

early to advanced stage (Fig. 2B). In three subsets of epithelial groups (Fig. 2C), hallmark pathway enrichment analysis of differentially expressed genes (DEGs) was performed (Fig. 2D). MYC and E2F target pathways stood out in C15-Epi as compared to C1-Epi and C14-Epi in both early and advanced stage (Fig. 2D and supplementary Fig. 4C). MYC plays a central role in proliferation and survival pathway while ERK and PIK3 cascades are known to stabilize MYC via phosphorylation [24, 25]. To integrate mouse and human data, we analyzed the gene expression of Kras and Myc-related genes in mouse epithelial cells. This analysis revealed that the mouse E2 subset also exhibits Myc-related gene expression (Supplementary Fig. 4D). Therefore, we hypothesize that C15-Epi in human PDAC resembles E2 in the mouse model of Kras-mutated PanINs (Fig. 1D).

Since ERK activity is tightly controlled by the family of DUSPs, we thus investigated family members of DUSP. Dotplot analysis showed that DUSPs are highly abundant in immune cells while various expression levels of DUSP1, DUSP2, DUSP4, and DUSP6 were observed across different cell types (Fig. 2E). Further analysis of DUSP expression in epithelial subsets revealed that only the level of DUSP2 were reduced in C15-Epi at the advanced stage, suggesting the up-regulated ERK activity may be due to DUSP2 loss (Fig. 2F). As a proof of concept, transfection of DUSP2 in PANC-1 pancreatic cancer cells decreased ERK activity which was not affected by phosphatase dead DUSP2; conversely, knockdown of DUSP2 increased ERK phosphorylation (Fig. 2G). The in vitro data were further supported by genetically engineered mouse model. In Kras-mutated background, knockout of Dusp2 ($Kras^{LSL-G12D/+}$, $Dusp2^{fl/fl}$, $Pdx1^{Cre/+}$, KDC) resulted in formation of more severe pancreatic lesion with less apoptotic cells when compared to Kras mutated ($Kras^{LSL-G12D/+,}$ $Pdx1^{Cre/+}$, KC) pancreas at the same age (Fig. 2H). Together, these results suggest that alteration of DUSP2 expression is sufficient to regulate ERK activity, and Dusp2 suppression may provide survival advantages in the background of Kras mutation.

ERK activity and DUSP2 expression is regulated in pancreatic cancer cells when interacting with differentiated monocytes

Results of scRNA sequencing performed in mouse and human pancreatic tissues revealed that macrophage population is markedly enriched from early to late stage of pancreatic cancer microenvironment (Fig. 3A), we therefore investigate the possibility of macrophages in regulating ERK activity in pancreatic cancer cells. To demonstrate the effect of macrophages, conditioned media from monocyte, macrophage, and human pancreatic stellate cells (progenitor of pancreatic fibroblast) were collected and used to treat PANC-1 pancreatic cancer cells. Treatment with macrophage conditioned medium (MCM) but not monocytes or pancreatic stellate cells conditioned media resulted in increasing ERK phosphorylation and reducing DUSP2 expression (Fig. 3B and supplementary Fig. 5A). Interestingly, despite conditioned medium from monocyte failed to induce ERK phosphorylation, co-cultured of monocytes with cancer cells for 3 days resulted in reducing DUSP2 expression and enhancing ERK activity (Fig. 3C and supplementary Fig. 5B-C). These results suggest ERK/DUSP2 axis is regulated as cancer cells and monocytes mutually interact. Indeed, co-culture with cancer cells induced attachment and differentiation of U937 monocytic cells and $CD14^{+}$ PBMC from healthy donors (supplementary Fig. 5D and Fig. 3D). To mimic the interaction of pancreatic cancer cells and macrophages in the microenvironment, monocyte was first differentiated into macrophage and co-cultured with PANC-1 cells for 48 h. The result of Western blotting showed that ERK was activated and DUSP2 was decreased in PANC-1, AsPC-1, and MIA PaCa-2 cells when co-cultured with macrophages (supplementary Fig. 5E). We further evaluated the change of ERK and DUSP2 over time, we observed that ERK was rapidly activated and sustained for at least 2 days after MCM treatment, while the reduction of DUSP2 was detected after ERK activation (Fig. 3E). Furthermore, treatment with ERK inhibitor (SCH772984) reversed MCM-induced cell morphology changes and the reduction of DUSP2 (Fig. 3F). These results imply that ERK activation by MCM results in a reduced level of DUSP2, thus preventing ERK inactivation by DUSP2. To demonstrate the correlation of DUSP2 loss, ERK activity, and macrophage infiltration in facilitating PDAC progression, wild type, KC and KDC mice pancreata were subjected to immunohistochemical staining. It can be observed in Kras-mutant lesions that ERK1/2 phosphorylation region correlates with advanced status and are surrounded by macrophages (stained by F4/80 antibodies) but not naïve monocyte (stained by antibodies raised against blood monocyte components, Mac), and Dusp2 knockout have enhanced pERK and surrounding macrophages (Fig. 3G and supplementary Fig. 5F-5G). Together, these data suggest monocytes differentiate into macrophages after interacting with tumor cells and differentiated macrophages are capable of inducing prolonged ERK activation in pancreatic cancer cells.

$ERK^{active}DUSP2^{low}$ axis in pancreatic cancer cells suppresses E-cadherin and promotes metastatic ability

PANC-1 cells treated with MCM for 24 and 48 h showed morphological changes with spindle-like appearance (supplementary Fig. 6A), indicating cells are undergoing epithelial-mesenchymal transition. In contrast, PANC-1 cells treated with control medium or monocyte

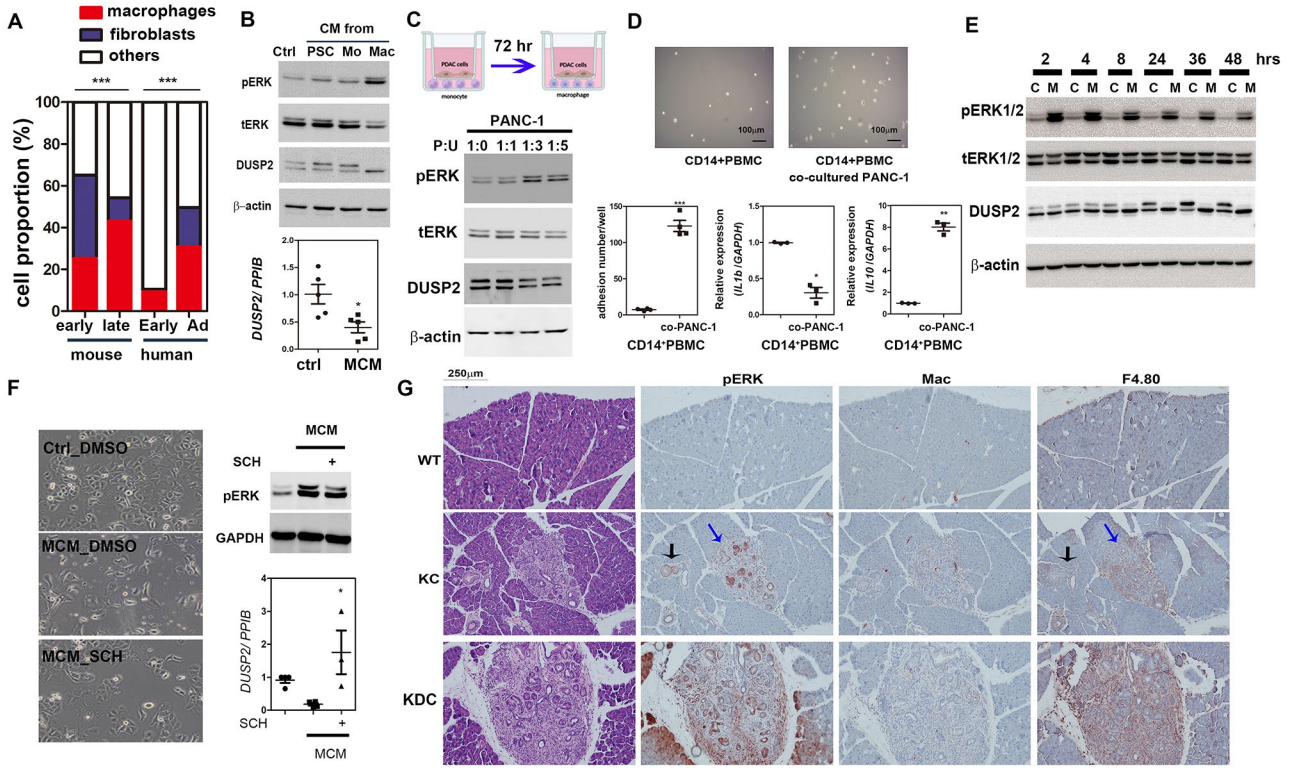

Fig. 3 Macrophage induces ERK phosphorylation in pancreatic cancer cells. (**A**) The proportion of macrophages, fibroblasts, and other types of cells in scRNA sequencing performed in mouse and human pancreatic tissue. Chi-square analysis was performed to compare the number of macrophages in mouse and human scRNA-seq data in their distribution between early and advanced disease statuses. (**B**) Western blot (upper) result shows the expression of ERK1/2 phosphorylation (pERK), total ERK1/2 (tERK), DUSP2, and β-actin in PANC-1 cells treated with control medium (Ctrl) or conditioned medium (CM) from human pancreatic stellate cells (PSC), U937 (undifferentiated naïve monocyte Mo), and macrophages (Mac) for 48 h. RT-qPCR (lower) for the expression of DUSP2 in control and macrophage-CM (MCM) treated PANC-1 cells. (**C**) Illustration of the co-culture system of PANC1 cells with monocytes (U937) by Transwell for 72 h (upper). The expression of DUSP2, pERK, tERK, and β-actin was detected in PANC-1 co-cultured with different ratio of U937. (**D**) Attachment of CD14 + PBMCs to tissue culture plate after co-culture with PANC-1 cells. Quantification of number of attached CD14 + PBMCs cells after co-culture with PANC-1 cells for 3 days (left). qRT-PCR for gene expression of *IL1B* and *IL10* in CD14 + PBMCs cells and CD14 + PBMCs co-cultured with PANC-1 cells for 3 days (right). (**E**) Western blot result shows the expression levels of pERK1/2, tERK1/2, and DUSP2 in control and MCM treated PANC-1 cells in different time points. (**F**) PANC-1 cell morphology of control, MCM treated, and MCM plus ERK inhibitor (SCH772984) treatment (left). Western blot (right, upper) and RT-qPCR (right, lower) showed the expression of DUSP2 is reversed if treated with ERK inhibitor (SCH772984). (**G**) Representative histology and immunohistochemical staining images (serial section) show expression of phosphorylated ERK1/2 (pERK), monocyte/macrophage (Mac) and macrophage (F4/80) in the lesion of KC ($Kras^{LSL-G12D/+}$, $Pdx1^{Cre/+}$), and KDC ($Kras^{LSL-G12D/+}$, $Dusp2^{fl/fl}$, $Pdx1^{Cre/+}$) transgenic mouse compared to pancreata in control mice

conditioned medium remained polygonal shape (supplementary Fig. 6A). Live cell imaging monitoring of cell movement showed that PANC-1 cells became more motile under MCM treatment as compared to those treated with control media (Fig. 4A). MCM induced ERK phosphorylation and cell migration can also be observed in another pancreatic cancer cell line MIA PaCa-2 but not in the normal epithelial ductal (HPDE) cells (supplementary Fig. 6B-C). Due to the changes in morphology and migration ability, we thus detected the expression of some structural proteins. First, analysis of a publicly available dataset comparing PANC-1 and macrophage co-cultured PANC-1 [26] showed the enrichment of structural organization pathway (Fig. 4B). Western blotting results indicated that E-cadherin was significantly decreased by MCM while no noticeable difference in ZO-1 or Vimentin expression (Fig. 4C). We next investigated whether E-cadherin suppression by MCM is due to ERK activation. Treatment with MEK inhibitor (U0126) and selective ERK1/2 inhibitor (SCH772984) inhibited ERK phosphorylation and reversed E-cadherin protein expression (Fig. 4D and supplementary Fig. 6D). E-cadherin is well-known to be repressed at transcriptional level via transcription factors (family of ZEB, Snail, or Twist), by which interacts with co-repressor C-terminal binding protein (CtBP). CtBP bridges transcription factors to chromatin remodeling enzyme and silences target genes. Indeed, the interaction of CtBP with HDAC1 and HDAC2 was further enhanced in MCM-treated cells measured by proximal ligation assay (Fig. 4E) even though the binding of CtBP to E-cadherin promoter is at similar level in control and MCM-treated PANC-1 cells

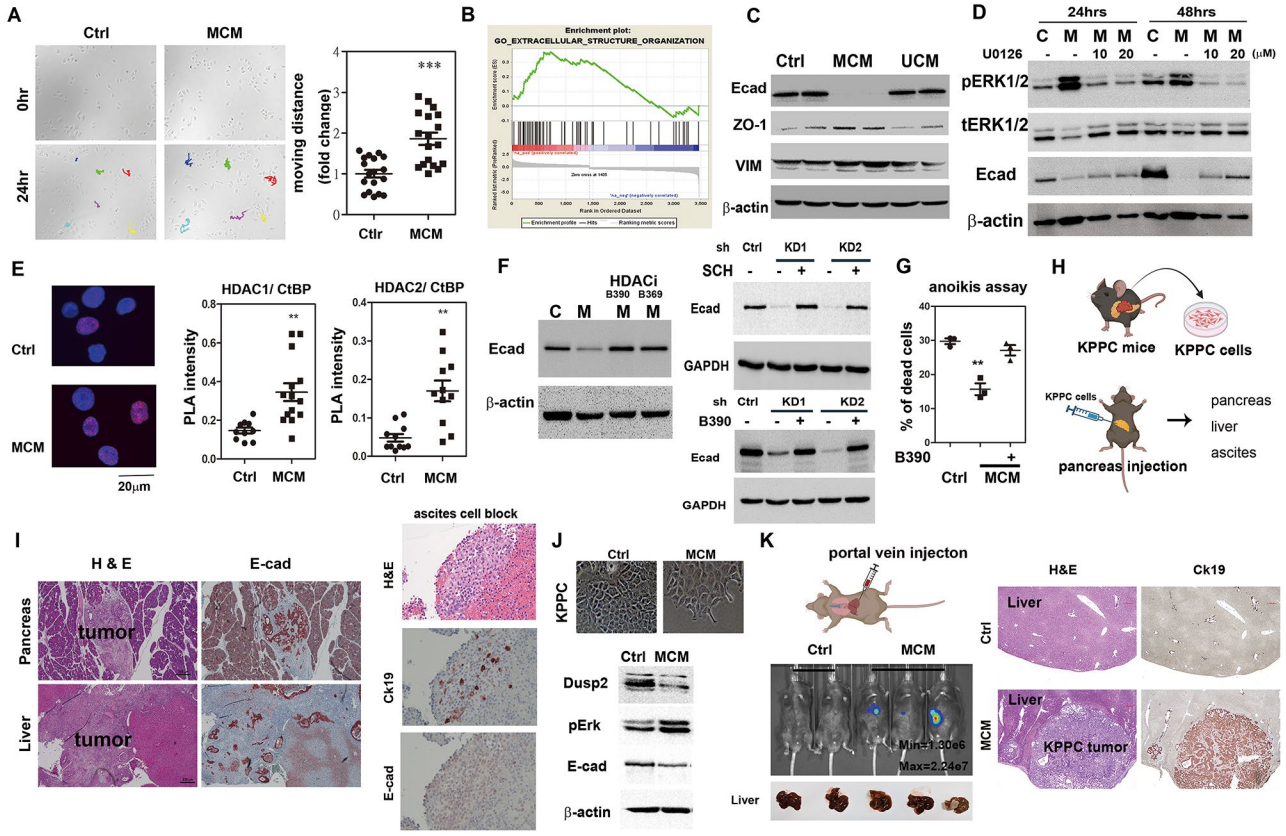

Fig. 4 MCM epigenetically suppresses E-cadherin expression and promotes metastasis. (**A**) Control and MCM treated PANC-1 cells were plated in petri dish and recorded by live cell imaging (JuLiBr, supplementary movie 1). The images were taken every 10 min in a total of 24 h. The track of sequence image was measured and quantified by ImageJ (right panel). Analysis was derived from results of three independent experiments with six cells of each time. (**B**) Analysis of gene sets (GSE109110) comparing PANC-1-co-cultured TAMs vs. PANC-1-alone control indicates the enrichment of extracellular/structure signature. (**C**) Representative Western blot results show the expression of E-cadherin, ZO-1, Vimentin and β-actin in control, MCM or UCM treated PANC-1 cells. (**D**) PANC-1 cells were pre-treated with MEK inhibitor (U0126) for 15 min and then treated with MCM for 24 and 48 h. Representative western blot results show the expression of pERK, E-cadherin, ERK and β-actin. (**E**) Proximity ligation assays (PLA) was performed to detect the HDAC1-CtBP and HDAC2-CtBP interaction Representative image (left) and quantification (right) was shown. (**F**) Suppressed E-cadherin is restored if HDAC inhibitor (B369 and B390) was employed (left). DUSP2-KD PANC-1 cells were treated with HDAC or ERK inhibitor and MCM for 24 h. Whole cell lysate was collected for the detection of E-cadherin and GAPDH. (**G**) Control, MCM, and MCM plus HDAC inhibitor treated PANC-1 cells were plated in low-attachment plate for 24 h. Annexin V positive cells were measured by flow cytometry. (**H**) Illustration of the isolation of KPPC cells and experimental design. KPPC cells were injected into the pancreas of immunocompetent mice. After one month of injection, pancreas, liver, and ascites were collected for further analysis. (**I**) H&E stain and immunohistochemistry staining for E-cadherin in pancreas, liver, and ascites blocks of mice injected with KPPC cells. Mice harbor KPPC tumors develop ascites which were pelleted and processed for cell block. H&E stain and immunohistochemistry staining for E-cadherin and Ck19 in the ascites cell block. (**J**) KPPC cells treated with MCM showed morphology change (upper), and decreased Dup2 and E-cadherin, and increased pERK measured by Western blotting (lower). (**K**) KPPC cells labeled with luciferase were injected into mice via portal vein. IVIS imaging was used to track the development of liver metastases in mice. After one month, mice were sacrificed and livers were taken (left). H&E stain and immunohistochemistry staining for Ck19 expression in the liver of mice injected with control or MCM-treated KPPC cells (right)

(supplementary Fig. 6E). Consistently, treatment with selective HDAC1/2 (B390) or ERK inhibitor prevented E-cadherin suppression by MCM and reversed E-cadherin in AsPC-1 and DUSP2-KD cells (supplementary Fig. 6F and Fig. 4F), supporting the idea that ERK phosphorylation mediates E-cadherin repression via HDAC/CtBP interaction.

ERK1/2 phosphorylation is tightly controlled by DUSP2, we next examined whether loss-of-DUSP2 in pancreatic cancer cells recapitulate MCM-induced molecular and cellular phenotypes. Similar to MCM treatment, DUSP2 knockdown (DUSP2-KD) cells show spindle-like morphology compared to polygonal shape of control cells. Live imaging demonstrated that DUSP2-KD cells display increased moving speed and distance compared to control cells (supplementary Fig. 6G). E-cadherin mRNA and protein expression were decreased in DUSP2-KD cells compared to control (supplementary Fig. 6H-I). Lastly, immunohistochemistry staining showed reduced E-cadherin expression in DUSP2-KD-inoculated orthotopic tumor as compared to control tumor (supplementary Fig. 6J). Together, these results

suggest that DUSP2 knockdown shows similar phenotypes as MCM treatment.

Loss of E-cadherin is highly associated with acquired anchorage independent ability of cancer cells. MCM-treated PACN-1 cells have increased anoikis resistance which was abolished if pre-treated with HDAC1/2 inhibitor (Fig. 4G), suggesting MCM-repressed E-cadherin in pancreatic cancer cells provide survival advantage after detachment. KPPC cells, isolated from pancreatic cancer of KPPC transgenic mousse ($Kras^{LSL-G12D/+}$, $Trp53^{LSL-R172H/R172H}$, $Pdx1^{Cre/+}$) were injected back to pancreas of same genetic background, immune competent mice (Fig. 4H). KPPC cells formed very aggressive tumors and mice often develop ascites and morbid within one month. E-cadherin was expressed in the cancer in-situ and liver metastasis but was markedly reduced in the cancer cells disseminated to the peritoneal cavity (Fig. 4I). Similar to human PANC-1 cells, murine KPPC cells treated with MCM expressed reduced Dusp2 and E-cadherin with enhanced Erk1/2 phosphorylation (Fig. 4J). To directly evaluate the metastatic ability, very low number of KPPC (10,000) cells were injected via portal vein and tracked by IVIS imaging. As compared to parental KPPC injected mice, MCM-educated KPPC cells were able to develop liver metastases (Fig. 4K). These results provide evidence to show that MCM-selected pancreatic cancer cells have acquired the capacity to accomplish the process from intravasation to colonization.

$ERK^{active}DUSP2^{low}$ cells exacerbates macrophage-mediated cancer malignancy

Multiple factors necessitate the successful establishment of distant metastases. To investigate whether macrophages-educated pancreatic cancer cells acquire other abilities in the tumor microenvironment, we analyzed cell communication and signaling pathways involved in the transition from early to late Kras mutated pancreas. Overall interaction strength and numbers are increased in the late Kras mutated tumors while enhanced incoming and outgoing signals from macrophages-ductal cells are also observed (Fig. 5A and supplementary Fig. 7A). We next performed orthotopic injection of parental PANC-1 cells and the MCM-selected pooled population into pancreas of mice. The tumor mass of MCM-selected pool population was bigger than the control group visually (Fig. 5B). In addition, two out of six mice injected with MCM-selected PANC-1 cells developed liver metastasis (Fig. 5B). Consistent with the in vitro result, E-cadherin remained suppressed in MCM tumors (Fig. 5B). Cell-chat signaling analysis indicated an increase in VEGF signaling and the participation of macrophages (Fig. 5C and supplementary Fig. 7B). Immunohistochemistry staining revealed that lymphangiogenesis ($Lyve\text{-}1^+$) but not angiogenesis ($CD31^+$) process was enhanced in MCM-selected tumors (Fig. 5D). The observation was supported by in vitro data as MCM-treated PANC-1 cells increased VEGF-C expression, which was inhibited by co-treatment with ERK inhibitor (Fig. 5E). Similarly, knockdown of DUSP2 increased VEGF-C expression in PANC-1 cells and the induction can be further amplified by co-cultured with macrophages (Fig. 5F), suggesting macrophages augment $ERK^{active}DUSP2^{low}$ cancer cells-mediated lymphangiogenesis.

Although lymphangiogenesis can be a route for tumor cells to metastasize, it also promotes T cell infiltration [27, 28]. In human PDAC, T cell population constitutes 54% in total cell population in the early stage and cytotoxic T cells ($CD8^+$, defined as $CD8^+GZMA/B^+$) made up one-third of total T population (supplementary Fig. 7C). Therefore, without the ability to escape from immune surveillance, tumor cells may not accomplish metastasis. Indeed, cell-chat analysis revealed the upregulation of programmed death ligand-1 (PD-L1) signaling in late KIC tumors (Fig. 5C), suggest that tumor cells evolve a strategy for immune escape. The expression of PD-L1 (encoded by CD274) is increased in DUSP2-KD cells, and a further enhancement was detected if co-cultured with macrophages (Fig. 5G). Finally, we utilized cancer cells derived from KPPC mouse to demonstrate the immune escape of macrophage-educated cancer cells. Co-cultured with U937 induced ERK phosphorylation and PD-L1 expression in KPPC cells (Fig. 5H), which prevents them from being killed by freshly isolated mouse splenocytes (Fig. 5I). Together, these results imply that interacting with macrophages enables $ERK^{active}DUSP2^{low}$ cancer cells to escape T cell-mediated cytotoxicity.

$ERK^{active}DUSP2^{low}$ signaling is prolonged by TIMP-1-CD63 axis

To dissect by which factor from macrophages maintains $ERK^{active}DUSP2^{low}$ status in pancreatic cancer cells, we performed further analysis of macrophages in human PDAC. Macrophages were clustered into three groups based on some commonly used pro- or anti- inflammation markers (supplementary Fig. 8A). To investigate the mutual communication between $ERK^{active}DUSP2^{low}$ epithelial cells and macrophages, CellChat analysis was performed. It was observed that C15-Epi shows an enhanced outgoing signal to C4 and C9-macrophage during the progression from early to advanced stage (Fig. 6A). Interestingly, C15-Epi also receives incoming signals from C9-Mac as compared to C1-Epi and C14-Epi (Fig. 6B). Therefore, we infer that C9-Mac and C15-Epi have mutual interaction. Notably, all three macrophage subpopulations are increased in the advanced tumors as compared to early stage tumor and C9-Mac population shows the most significant change (supplementary Fig. 8B). Gene expression analysis in three subsets of

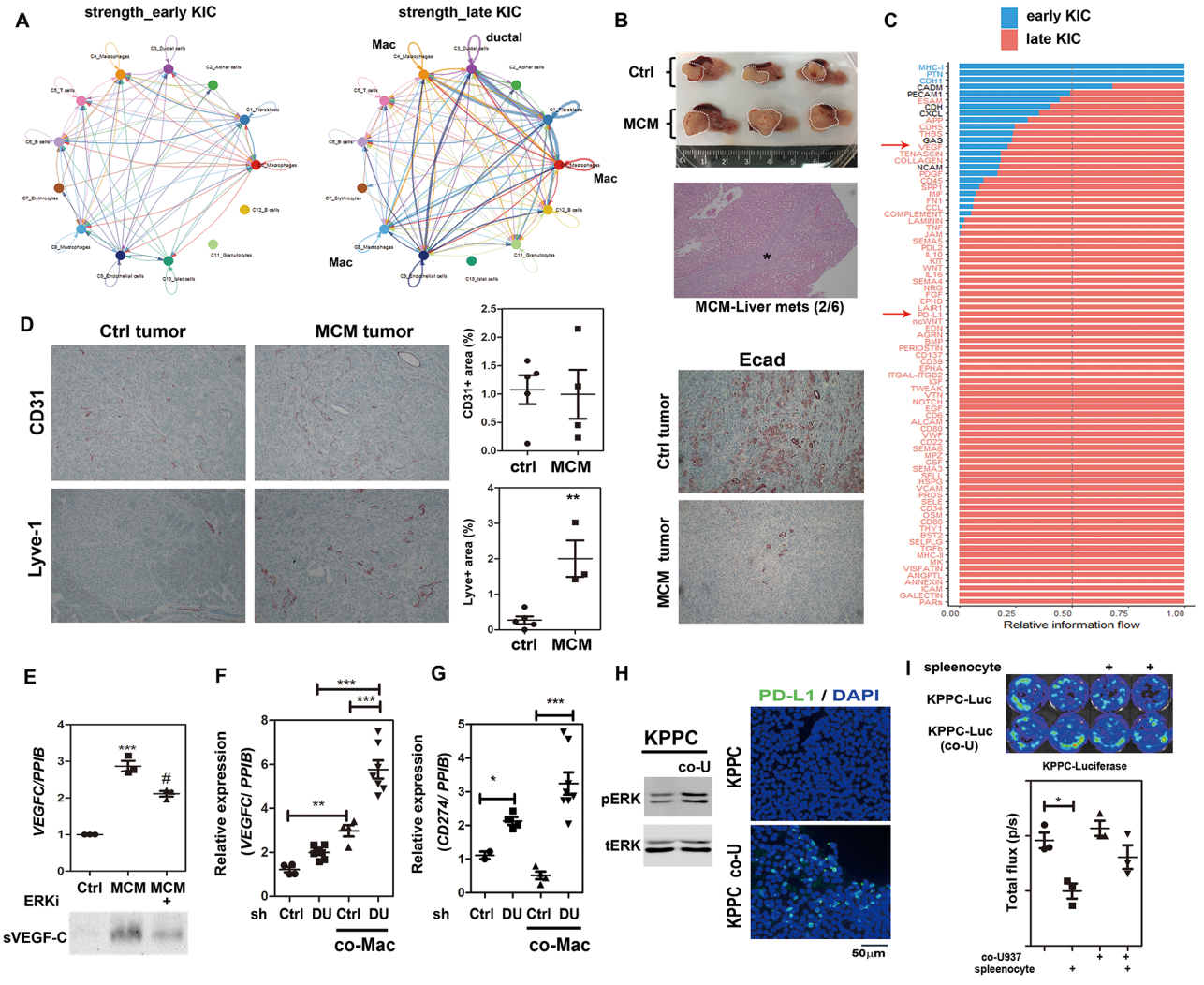

Fig. 5 Macrophage exacerbates ERK^{active}DUSP2^{low} mediated lymphangiogenesis and immune escape. (**A**) Cellchat analysis for cellular communication among distinct cell populations in early and late KIC pancreas. Circle plot was served as visualization outputs and different colors represent different cell groups. (**B**) Picture of pancreatic tumors developed from SCID mice orthotopically injected with control or MCM-selected PANC1. The dotted lines show tumor mass. H&E stain of mouse liver from MCM-selected PANC-1 group. The asterisk indicates tumor mass. Numbers of mice with metastatic lesions and total numbers of mice in MCM-selected PANC-1 group is indicated at the bottom of micrographs (upper). IHC staining showed the expression of E-cadherin in control or MCM-selected pancreatic tumors (lower). (**C**) All the significant signaling pathways in early and late KIC were ranked based on their differences of overall information flow. The overall information flow of a signaling network is calculated by summarizing all the communication probabilities in that network. The top signaling pathways colored by red are more enriched in late KIC, and the pathways colored by blue were more enriched in the early KIC pancreas. (**D**) IHC staining for LYVE-1 and CD31 in control or MCM-selected pancreatic tumors (left). Quantification of LYVE-1 and CD31 in control and MCM-selected pancreatic tumors (right). (**E**) The expression of VEGF-C in control, MCM, MCM plus ERK inhibitor treated PANC-1 cells measured by RT-qPCR (upper) and Western blotting (lower). (**F**) RT-qPCR for VEGF-C expression in control and DUSP2-KD PANC-1 cells co-cultured with macrophages for 2 days. (**G**) RT-qPCR for the expression of PD-L1 (*CD274*) in pancreatic cancer cells. U937 cells were first differentiated into macrophages and co-cultured with control or DUSP2-KD PANC-1 cells for 2 days. (**H**) KPPC cells co-cultured with U937 for 5 days showed increased ERK phosphorylation (left). Immunocytochemistry for PD-L1 expression in KPPC and KPPC which has been co-cultured with U937 (right). (**I**) Total flux was determined to represent cell numbers of KPPC cells which are luciferase labeled. KPPC cells were first co-cultured with U937 for 5 days and then incubated with freshly isolated mouse splenocytes for 2 days

macrophages revealed many shared pathways with the notable exception of "protein secretion", which was specifically enhanced in the C9-Mac subset at the advanced stage (Fig. 6C and supplementary Fig. 8C). To identify factors secreted from macrophages that causes ERK^{active}-DUSP2^{low} phenomenon in pancreatic cancer cells, we performed cytokine array assay in macrophage conditioned medium and identified several potential targets (Fig. 6D). After excluding the involvement of well-known cytokines such as IL8, IL10, and CXCL10-mediated signaling via co-treatment of MCM with inhibitors of corresponding receptors (supplementary Fig. 8D), we

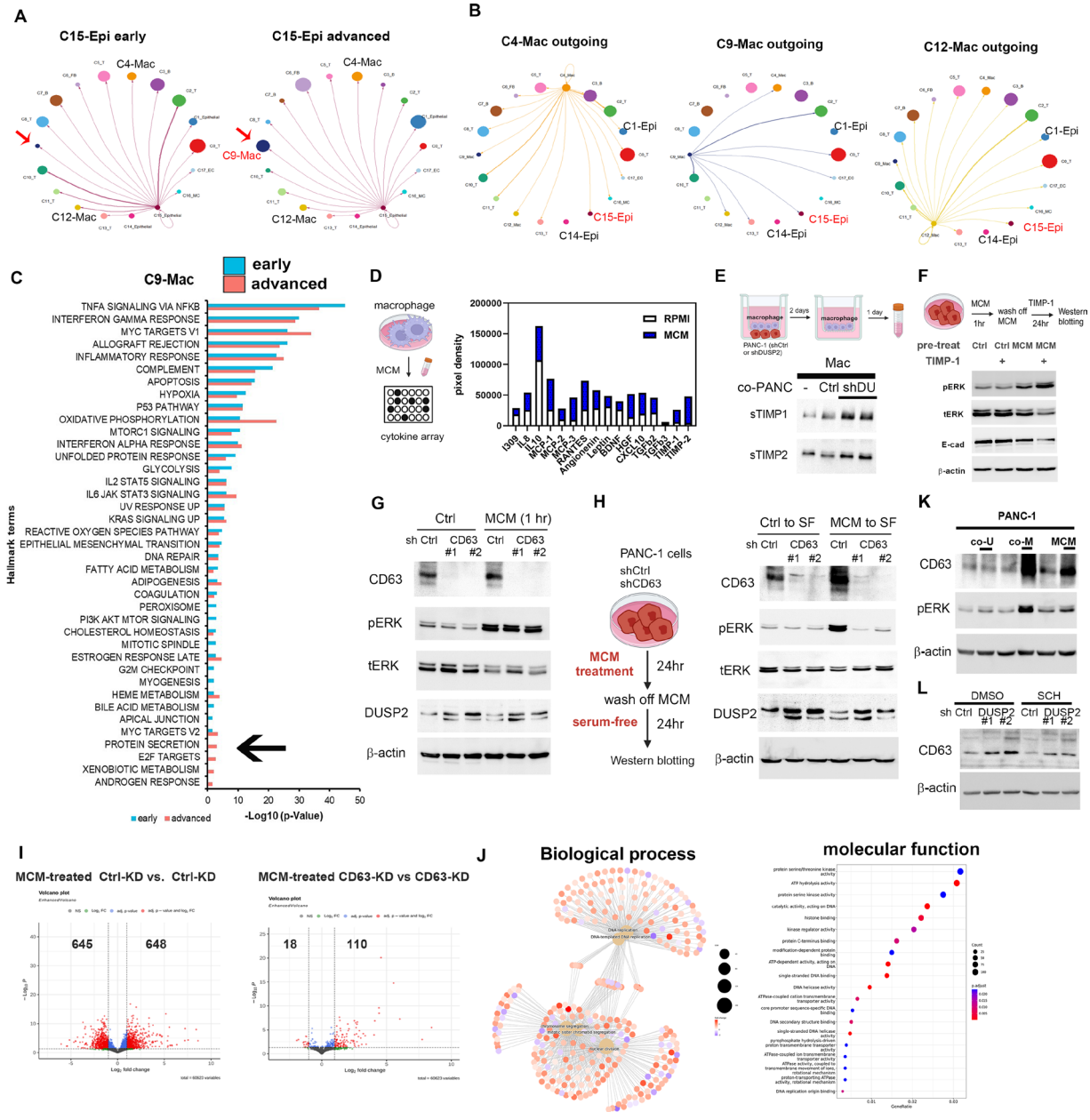

Fig. 6 Decipher the signaling interaction between macrophage and ERK^{active}DUSP2^{low} epithelial cells. (**A**) Circle plot showing the inferred signaling networks from C15-Epi subset toward subsets of other epithelial, macrophage and T cells in early and advanced stages. The round loops along with cell type represent the interactions within the same cell type. (**B**) Circle plots showing the outgoing signals from each macrophage subset (C4, C9, and C12) in the early PDAC. (**C**) Hallmark pathway enrichment analysis of DEGs in C9-Mac in early and advanced PDAC tumor. (**D**) Cytokine array (RayBiotech) was used to identify potential factors secreted from macrophage (MCM) compared to RPMI which contains 10% FBS. (**E**) The expression of TIMPs in macrophages. Macrophages were first co-cultured with PANC-1 for 2 days and then cultured alone by serum-free RPMI medium for an additional day. Conditioned medium was collected and concentrated to measure the expression of TIMP-1 and TIMP-2 by Western blotting. (**F**) PANC-1 cells were initially treated with MCM for 1 h, after which they were cultured in serum-free medium with or without recombinant TIMP-1 (Peprotech) for 24 h. Western blotting was then performed to assess the expression of DUSP2, pERK, E-cadherin, and β-actin. (**G**) The expression of CD63, pERK, tERK, DUSP2, and internal control β-actin in control and CD63 knockdown (KD) PANC-1 cells after being treated with MCM for 1 h. (**H**) Control and CD63-KD PANC-1 cells were first treated with or without MCM for 24 h and the medium was replaced by serum-free RPMI for an additional 24 h. The expression of CD63, pERK, tERK, DUSP2, and internal control β-actin was determined by Western blotting. (**I**) The volcano plot illustrates the number of genes that are significantly upregulated or downregulated in MCM-treated cells compared to untreated cells under both Ctrl-KD and CD63-KD conditions, with a fold change greater than 2. (**J**) GO analysis was conducted on differentially expressed genes comparing MCM-treated Ctrl-KD and MCM-treated CD63-KD cells, focusing on their involvement in biological processes and molecular functions, as illustrated in cnetplots and dotplots. (**K**) The expression of CD63, pERK, and internal control β-actin in PANC-1 cells that have been co-cultured with monocyte (co-U) for 3 days, with macrophage (co-M) for 2 days, or treated with MCM for 2 days. (**L**) The expression of CD63 and β-actin in control and DUSP2-KD PANC-1 cells treated with DMSO or ERK inhibitor (SCH772984)

narrowed down the potential candidates to TIMPs. Both TIMP-1 and TIMP-2 have high expression in MCM or secreted from macrophages, while the expression of TIMP-1 but not TIMP-2 was further increased if macrophages have been co-cultured with PANC-1 (Fig. 6E). An increase in TIMP-1 was also observed in macrophages co-cultured with various pancreatic cancer cells (supplementary Fig. 8E). Unexpectedly, the effect of recombinant TIMP-1 was not profound unless the cells had been pretreated with MCM (Fig. 6F), suggesting TIMP-1 may play a role in extending or prolonging the phosphorylation of ERK. To determine whether CD63, a direct cell surface receptor of TIMP-1 [29], mediates MCM-induced effect, CD63 was knocked down (CD63-KD) in PANC-1. Treatment with MCM for 1 h induced ERK phosphorylation in both control and CD63-KD PANC-1 cells (Fig. 6G), suggesting the rapid induction of ERK is not mediated via TIMP-1-CD63 signaling. While ERK is activated by 24 h MCM treatment in both control and CD63-KD PANC-1 cells, ERK activity is significantly subsided in CD63-KD cells when exposed to a lower concentration of MCM (supplementary Fig. 8F), implying the cancer cells are less responsive to MCM when CD63 expression is suppressed. Furthermore, MCM-induced ERK phosphorylation was maintained in the control but not CD63-KD cells after washing off MCM for 24 h (Fig. 6H), suggesting that TIMP-1-CD63 signaling mediates the prolonged activation of ERK. Next-generation RNA sequencing of control-KD and CD63-KD PANC-1 cells under MCM-treated and untreated conditions revealed that the number of differentially regulated genes (either upregulated or downregulated) is significantly reduced in response to MCM induction when CD63 expression is suppressed (Fig. 6I). The GO analysis of differentially regulated genes indicated that the involvement of genes associated with DNA replication, mitosis, and protein serine/threonine kinase activity was lost in the CD63 knockdown cells following MCM treatment (Fig. 6J). As cell cycle regulation is one of the major pathways regulated by ERK in KRAS-mutated PDAC [25, 30], these data further support our assertion that CD63 is critical for mediating pancreatic cancer cells' responses to macrophage induction via sustained ERK activity. It was observed that the expression of CD63 in cancer cells is increased after treatment with MCM or co-cultured with macrophage but not naïve monocyte (Fig. 6K), and the increased CD63 in DUSP2-KD cells is ERK activity-dependent (Fig. 6L). Furthermore, the level of DUSP2 is upregulated in CD63-KD cells, suggesting that CD63-mediated signaling may negatively regulate DUSP2. Together, our results suggest that TIMP-1-CD63 signaling is critical in sustaining ERK activity and repressing DUSP2 expression in pancreatic cancer cells. TIMP-1 level is increased in macrophages while CD63 expression is enhanced in cancer cells during their mutual interaction, creating a perpetuating cycle.

Clinical correlation between TIMP-1 and CD63 interaction in PDAC cohort

Lastly, we aimed to demonstrate the critical epithelial-macrophage interaction in human PDAC samples. Tissues of human PDAC were obtained and processed for nanostring digital spatial profiling (Fig. 7A). Antibody targeting PanCK and CD45 were used to capture epithelium and immune cells and the expression of transcripts in selected regions of interest (ROIs) were analyzed by next-generation sequencing. xCell was used for the prediction of immune cell types in the ROIs, indicating that macrophage is the dominant population and the major source of TIMP-1 among immune cells (Fig. 7B). Also, TIMP-1 is highly expressed in the M2 macrophage (Fig. 7C) as characterized by gene signature defined by the xCell platform [31]. Correlation analysis revealed a positive correlation between TIMP-1, but not TIMP-2, in $CD45^+$ cells and CD63 in $PanCK^+$ cells (Fig. 7D), supporting the idea that there may be a positive regulatory relationship between TIMP-1 and CD63. A total of 97 pancreatic cancer samples were collected and bulk RNA sequencing was performed to establish our NCKUH cohort, which encompasses 100% adenocarcinoma cases with well-defined clinical stages (Table S1). The TCGA dataset was retrieved for comparison with the NCKUH cohort, and the clinical information is presented in Table S1. High TIMP-1 and high CD63 levels showed the worst disease-free survival (Fig. 7E) and can be considered with independent prognostic value based on the result of multivariate analysis (Table 1). Additionally, $TIMP1^{high}CD63^{high}$ correlates with M2 macrophage signature and pancreatic patient disease severity, including tumor stage, differentiated status, lymph node and liver metastasis, and chemotherapy response (Fig. 7F). At the gene expression level, $TIMP1^{high}CD63^{high}$ correlates with KRAS, VEGF-C, CD274 and M2 macrophage markers (CD163, MSR1, and MRC1)(Fig. 7F). Although $TIMP1^{high}CD63^{high}$ was not able to predict prognosis in the TCGA dataset, it reached statistical significance when grouped according to the M2 signature. Conversely, $TIMP1^{high}CD63^{high}$ in conjunction with the M2 signature displayed a greater risk in both univariate and multivariate analyses in the NCKUH cohort (Table 1). The analysis suggests that the role of TIMP1/CD63 axis may be more pronounced when associated with specific tumor microenvironment factors, such as the presence and influence of M2 macrophages. Together, clinical evidence illustrates the importance of $TIMP1^{high}CD63^{high}$ in affecting disease outcomes and corroborates the molecular mechanisms identified in our experiments.

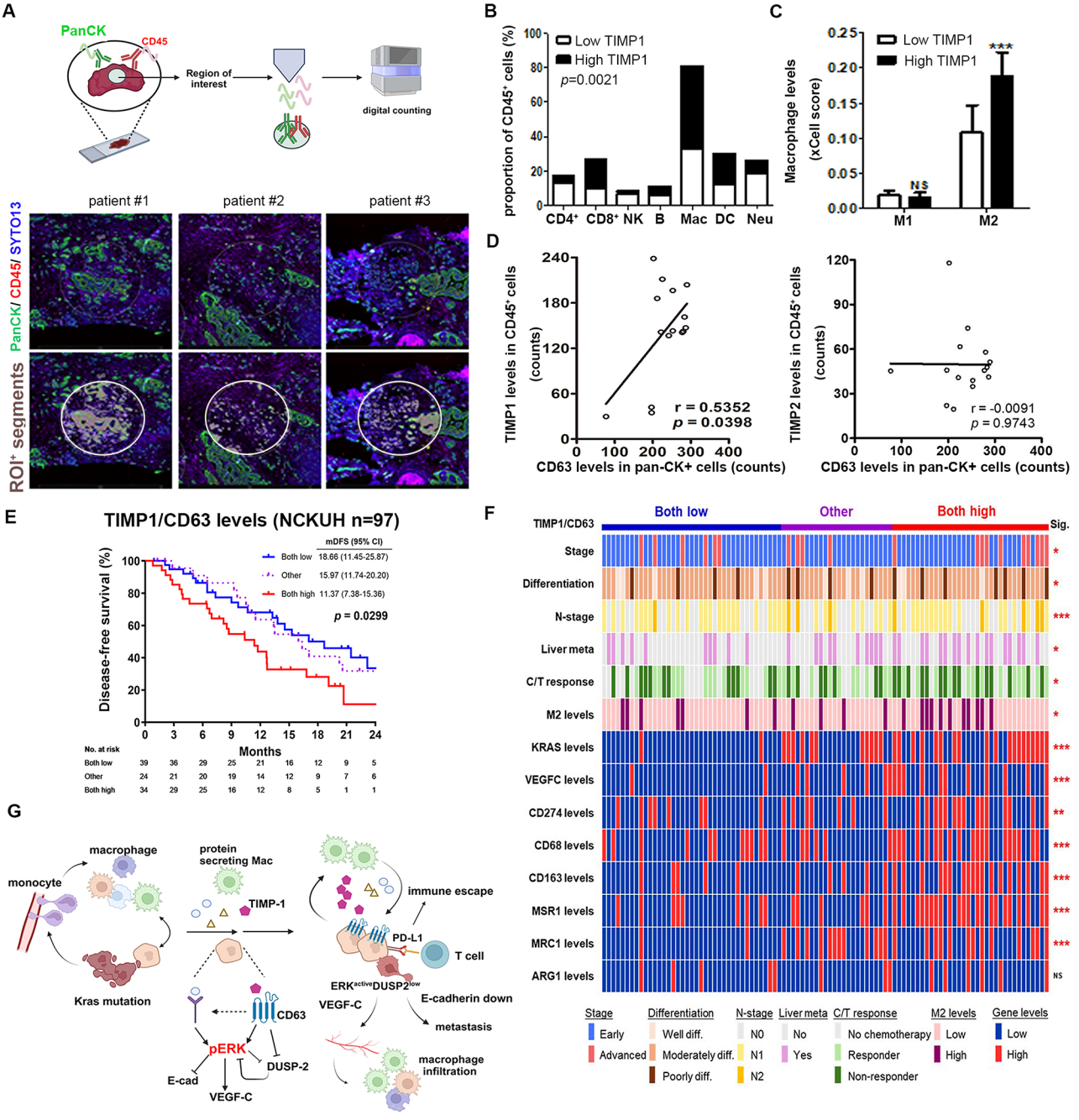

Fig. 7 The expression of Mac-TIMP-1 and Epi-CD63 predicts poor prognosis in PDAC. (**A**) The simple workflow of DSP. Antibodies covalently linked to DNA indexing oligonucleotide are used to stain tissue section. Several repeats of UV light liberates indexing oligonucleotide from the region of interest (ROI), and oligonucleotides are hybridized to NanoString fluorescent barcodes and quantified by NGS (NovaSeq 10B 150PE) (upper). Fluorescent imaging establishes the overall architecture of the tissue. Tissue-specific morphological features were highlighted by PanCK (green), CD45 (red) and SYTO13 (blue). PanCK, CD45, and SYTP13 identify epithelium, immune cells, and nucleic acid respectively. Representative ROI for PanCK and CD45 are shown (lower). (**B**) Cell-type enrichment analysis (xCell) was performed for the prediction of cell types within the $CD45^+$ population. (**C**) TIMP1 expression in M1 and M2 macrophage. M1 and M2 macrophages was predicted by webtool xCell. (**D**) Expression correlation between TIMP1 or TIMP2 in $CD45^+$ immune population and CD63 in $PanCK^+$ epithelial population. (**E**) Kaplan-Meier analysis of overall survival based on the expression of TIMP1 and CD63 levels in NCKUH cohort. (**F**) Waterfall plot (oncoplot) for the proportion of patient cases with disease status (stage, differentiation, lymph node, liver metastasis, chemotherapy response) in different levels of TIMP1/CD63. Others: $TIMP1^{high}CD63^{low}$ or $TIMP1^{low}CD63^{high}$. The mean value was used as the optimal cut-off values of TIMP1 and CD63. chi-square test was used for the correlation analysis. (**G**) A schematic illustration showing the interaction between macrophage and pancreatic cancer cells by the TIMP-1/CD63/ERK^{active} axis, and the leading consequence of the interaction. The working model was created in https://BioRender.com

Table 1 Univariate and multivariate analyses for disease-free survival

Factors	Univariate analysis		Multivariate analysis	
	HR (95% CI)	*P*	HR (95% CI)	*P*
NCKUH cohort				
Tumor stage (III + IV vs. I + II)	2.006 (1.111–3.625)	**0.021**	1.231 (0.612–2.478)	0.560
Liver metastasis (Yes vs. No)	5.183 (2.770–9.699)	**0.000**	5.396 (2.797–10.411)	**0.000**
Tumor grade (Moderately diff. vs. Well diff.)	1.134 (0.508–2.533)	0.759	1.248 (0.532–2.926)	0.610
Tumor grade (Poorly diff. vs. Well diff.)	2.683 (1.037–6.939)	**0.042**	1.913 (0.664–5.516)	0.230
TIMP1/CD63 (Only one high vs. Both low)	1.008 (0.523–1.942)	0.981	1.213 (0.612–2.403)	0.581
TIMP1/CD63 (Both high vs. Both low)	1.996 (1.099–3.626)	**0.023**	2.104 (1.084–4.086)	**0.028**
M2-high + TIMP1/CD63 (Only one high vs. Both low)	0.714 (0.112–4.549)	0.721	3.833 (0.373–39.384)	0.258
M2-high + TIMP1/CD63 (Both high vs. Both low)	6.170 (1.128–33.739)	**0.036**	19.828 (1.949-201.723)	**0.012**
TCGA cohort				
Surgical margins (R1 vs. R0)	1.803 (1.058–3.071)	**0.030**	0.982 (0.382–2.522)	0.970
Surgical margins (R2 vs. R0)	3.474 (1.222–9.876)	**0.020**	3.231 (0.818–12.761)	0.094
TP53 status (Altered vs. Unaltered)	2.294 (1.257–4.185)	**0.007**	1.762 (0.646–4.811)	0.269
M2-high + TIMP1/CD63 (Only one high vs. Both low)	1.114 (0.488–2.545)	0.797	1.031 (0.398–2.673)	0.950
M2-high + TIMP1/CD63 (Both high vs. Both low)	3.256 (1.275–8.312)	**0.014**	3.241 (1.194–8.798)	**0.021**

Abbreviations: HR, hazard ratio; CI, confidence interval; vs., versus

Bold values indicate statistically significant results

Discussion

Activating mutation of KRAS was observed in about 90% of PDAC; however, transgenic mouse study reveals that oncogenic Kras mutation initiates PanIN but inefficiently drives the progression to PDAC [3, 32], indicating additional stimulations are required to promote tumor malignancy. Indeed, we observed that PanIN lesions in Kras-mutated pancreas are also undergoing senescence and apoptosis (Fig. 1), suggesting that only a small proportion of Kras-mutated epithelial cells are able to develop into malignant cells. Herein, we demonstrate that mutual communication between a subset of cancer cells and infiltrated macrophages drives cancer cells to acquire proliferative, metastatic, and immune escaping abilities mediated by loss of DUSP2-induced prolonged ERK activation.

By analyzing single-cell RNA sequencing data from early and advanced stages PDAC samples, we noticed the increase of macrophage population in the advanced PDAC. Similar results were also observed by analyzing Kras mutated mouse pancreas single-cell RNA sequencing data [23]. Further analyses of macrophages and cancer epithelial cells identified two groups of cells (C9-macrophages and C15-epithelia) that deserve more attention. The enriched genes in epithelial cells of advanced stage PDAC are primarily E2F and MYC targets, indicating they are regulated by prolonged activation of ERK signaling. Since Kras activating mutation only causes transient but not prolonged ERK activation [3], we reason that the brake system that inactivates ERK signaling might be impaired in advanced-stage PDAC. We then analyzed the expression of DUSP1, 2, 4, 5, and 6 in different subsets of epithelial cells as they are phosphatases specifically for inactivating ERK. Interestingly, we found that DUSP2 was expressed in the C15-epithelial cells in the early-stage PDAC but was absent in the advanced-stage PDAC, which correlates with prolonged ERK activation. This indicates that DUSP2 loss may be a critical factor driving Kras-mutated epithelial cells to develop into malignant PDAC. Indeed, our data demonstrated that pancreas-specific knockout of Dusp2 in the Kras-mutated background facilitates PDAC lesion development.

We next aim to elucidate what causes the downregulation of DUSP2. During early development of cancer, monocytes are the first infiltrating population, and upon the stimulation of different cytokine or growth factors, they can further polarize into pro-inflammatory or pro-tumor macrophages [33, 34]. Our data show that co-cultured with pancreatic cancer cells stimulates $CD14^+$ PBMC and U937 monocytes to differentiate and express immune-suppressive cytokines implying that cancer cells educate infiltrated monocytes becoming pro-tumor macrophages. The in vitro results were mirrored by murine data as we identified the presence of macrophages in Kras-mutated pancreatic lesions, where increased ERK activity is observed. We reasoned macrophages may have a causal role in contributing to prolonged ERK signaling. Indeed, we found that conditioned medium from differentiated macrophages or monocytes co-cultured with cancer cells, but not naïve monocytes, causes ERK phosphorylation and DUSP2 downregulation in PANC-1 cells. Taken together, we show the interaction between cancer cells and infiltrated monocytes establishes an ERK^{active}-$DUSP2^{low}$ tumor microenvironment that may serve as a permissive signal to promote cancer progression.

PDAC has a propensity to metastasize at an early stage. Therefore, cancer cells may already acquire metastatic ability for subsequent metastasis during the early stage. E-cadherin, a transmembrane protein that mediates cell adhesion and polarization, is commonly observed downregulated in many cancers. Reduction of E-cadherin correlates with tumor stage, lymph node invasion, and distant metastases in pancreatic cancer [35–37]. Loss of E-cadherin expression was found in pancreatic circulating tumor cells [38], implying that downregulation of E-cadherin may be a prerequisite for metastasis. E-cadherin downregulation was observed in malignant pancreatic cancer cells after in vivo selection for three cycles [39]. However, in our study, we found that MCM quickly suppressed E-cadherin and the most intriguing part is that the downregulation is reversible (supplementary Fig. 9). This observation may be particularly important since the restoration of E-cadherin has been observed at metastatic site, implying the re-expression may be important for the colonization of metastases [40, 41]. Mechanistically, we demonstrated that MCM treatment downregulates E-cadherin is mediated via the binding of HDAC1/2 and the co-repressor, CtBP, to E-cadherin promoter. Our result is consistent with a previous study that showed ERK activation induces epigenetic silencing of E-cadherin via releasing the co-repressor CtBP from MCRIP1 [42]. Taken together, these results suggest that macrophage mediates $ERK^{active}DUSP2^{low}$ axis to downregulates E-cadherin expression via epigenetic mechanism, providing the advantage to accomplish metastasis from intravasation to colonization.

The development of cancer to an immune suppressive microenvironment should be considered as a dynamic and gradual process that is significantly influenced by cell-cell interaction. Since PDAC tumors encompass a large population of macrophages, their contribution to immune exclusion drew considerable attention. Emerging evidence suggests the phenotype of macrophages is reversible and TAMs have diverse functional status with both classically-activated M1 or alternatively-activated M2 features. Unbiased analysis revealed that there were three subsets of macrophages in the mouse model of pancreatic cancer [23]; similarly, in our cohort, three different subgroups of macrophages were segregated in human PDAC. Besides the observation that C9-Mac is the population that has mutual interaction with the ERK^{active}-$DUSP2^{low}$ epithelial cells (C15-Epi), we also observed that all three macrophages subsets have no outgoing signal to C14-Epi. Since C14-Epi has very low level of KRAS, suggesting that KRAS related signaling may be important for tumor cells to receive signals from macrophages. In contrast to C4-Mac and C12-Mac, C9-Mac does not express higher pro-inflammatory markers or anti-inflammatory markers (supplementary Fig. 8). However, the enrichment of protein secretion pathway in C9-Mac suggests the importance of an unidentified factor. Cytokine array has led to identifying various potential factors while we demonstrated that TIMP-1-CD63 signaling can be critical in sustaining ERK^{active} status. TIMPs are known for regulating activity of matrix metalloproteinases (MMPs) and their role in cancer progression has been gaining attention. In PDAC, emerging evidence indicated that TIMP-1 is associated with poor prognosis, functionally involved in perineural invasion [43] and liver metastasis [44]. In our study, macrophage co-cultured with PANC-1 have increased TIMP-1 expression while PANC-1 treated with MCM have enhanced level of its receptor CD63. Importantly, knockdown of CD63 abolished MCM-induced ERK activity, suggesting that TIMP-1-CD63 axis is central to the interaction between macrophage and pancreatic cancer cells. By spatial transcriptome analysis, we demonstrated the positive correlation between TIMP-1 in immune cells and CD63 in cancer cells. In bulk tumors of our NCKUH cohort, high levels of both TIMP-1 and CD63 are predictive of poor survival and demonstrating independent prognostic value. This suggests that while TIMP-1 alone may function as an MMP inhibitor, it can initiate tumor-promoting signaling when CD63 is co-expressed. Although $TIMP1^{high}/CD63^{high}$ expression does not show significant prognostic value in the bulk TCGA data, it becomes significant under M2 macrophage subgrouping conditions. This indicates the influence of M2 macrophages is crucial. The differing population backgrounds, including ethnic, clinical, and treatment variations, between the NCKUH and TCGA cohorts likely contribute to these differences, yet the underlying phenomenon remains essentially similar. Together, our results highlight the importance of TIMP-1-CD63 axis in directing tumor progression due to macrophage-cancer cell interaction.

Low infiltration of cytotoxic immune cells is one of the features of immune-excluded phenomenon in PDAC and serves as an indicator of reduced effectiveness of immunotherapy. Notably, single-cell analysis revealed that T cell population is abundant with a substantial presence of cytotoxic T cells in the early stage PDAC (Fig. 2B and supplementary Fig. 7). Programmed cell death protein 1 (PD-1, encoded by *PDCD1*) is an immune-inhibitory receptor expressed in activated T cells. If PD-1 is bound by the ligands (PD-L1/PD-L2), T cell function can be regulated toward reduced proliferation, decreased cytokine secretion or apoptosis. Our results showed that ERK^{active}-$DUSP2^{low}$ axis regulates PD-L1 expression in pancreatic cancer cells which can be further enhanced via mutual interaction with macrophages (Fig. 5). Taken together, our findings delineate the importance of interaction with macrophage in setting the $ERK^{active}DUSP2^{low}$ axis in pancreatic cancer cells, by which inhibits cytotoxic T-cell

function and dictates the development of an immune suppressive microenvironment.

By in vitro and in vivo experiments and analysis of clinical samples, we proposed a model (Fig. 7G). KRAS mutation in the epithelial/ductal population induces cell death and recruits immune cell infiltration. As monocytes differentiate into macrophages, they induce ERK activity in KRAS-mutated cells, and the reciprocal regulation starts. The action of macrophage-derived TIMP-1 leads to DUSP2 suppression and thus sustains ERK activity, inhibiting E-cadherin, and inducing metastatic ability of pancreatic cancer cells. On the other hand, ERK^{active}-$DUSP2^{low}$ cancer cells produce VEGF-C to stimulate lymphangiogenesis by which may expand immune cell infiltration. The expression of PD-L1 is also altered by the $ERK^{active}DUSP2^{low}$ axis via interaction with macrophages, which favors cancer cell survival and immune escape, thus contributing to the accomplishment of distant metastasis. Therefore, disruption of the vicious cycle between macrophage and pancreatic cancer cells may be a highly potential way to inhibit pancreatic cancer progression.

Conclusions

Our findings provide insight into the dynamic regulation in pancreatic cancer early development, highlighting that macrophage-epithelial cell communication confers survival advantages and promotes progression despite Kras-mutation-induced cell death and immune clearance. The establishment of the $ERK^{active}DUSP2^{low}$ axis in pancreatic cancer cells contributes to the evolution toward immune escape and metastasis. We revealed that TIMP-1-CD63 signaling sustains the vicious cycle between macrophages and pancreatic cancer cells, providing an alternative approach to target PDAC progression.

Abbreviations

DUSP2	Dual specificity phosphatase 2
ERK	Extracellular signal-regulated kinase
PDAC	Pancreatic ductal adenocarcinoma
PanIN	Pancreatic intraepithelial neoplasia
MCM	Macrophage conditioned medium
TAM	Tumor-associated macrophage
TIMP-1	Tissue inhibitor of metallopeptidase 1
scRNA-seq	Single-cell RNA sequencing
DSP	Digital spatial profiling

Supplementary Information

The online version contains supplementary material available at https://doi.org/10.1186/s12943-024-02207-4.

Supplementary Material 1

Supplementary Material 2

Acknowledgements

We like to thank Yi-Jou Chung and Yi-Hsuan Yeh for the technical support in immunohistochemistry staining. We like to thank Yi-Chen Tang for the technical support in animal experiments. We like to thank Yen-Yu Lai for the bioinformatics analysis. The authors are grateful for the support from the Core Research Laboratory, College of Medicine, National Cheng Kung University.

Author contributions

Conceptualization: CA Wang, YC Hou, YS Shan, SJ Tsai Methodology: CA Wang, YC Hou, YJ Tai, YK Hong, PC Hou, JL Fu Investigation: CA Wang, YC Hou, YJ Tai, YK Hong, C Shen Clinical sample preparation and processing: SM Cheng, DY Hwang, YY Su Histology evaluation: CL Wu Supervision: YS Shan, SJ Tsai Writing—original draft: CA Wang, SJ Tsai Writing—review & editing: CA Wang, YC Hou, YS Shan, SJ Tsai.

Funding

This work was supported by grants from National Science and Technology Council (NSTC), Taiwan (NSTC 112-2320-B-006 -031- for C-A W.; MOST 111-2326-B-006-002 for S-J T.; NSTC 112-2314-B-006-106, NSTC 112-2321-B-006-023, and NSTC 112-2321-B-006-010 for Y-S S.), Taiwan Ministry of Health and Welfare (MOHW, MOHW113-TDU-B-211-114008 and MOHW113-TDU-B-221-134015 for Y-S S.), National Health Research Institute (NHRI-EX112-11016BI for S-J T.), and National Cheng Kung University Hospital (NCKUH-11209005 for Y-S S.).

Data availability

scRNA raw data will be uploaded to GEO dataset and the other data that support the findings of this study are available from the corresponding author upon reasonable request.

Declarations

Ethical approval

Experimental procedures of animal studies were approved by the Institutional Animal Care and Use committee at the National Chung Kung University. Tumor specimens were obtained from PDAC patients undergoing surgical resection at the National Cheng Kung University Hospital (NCKUH) under Institutional Review Board (IRB)-approved protocol (IRB number: NCKUH B-ER-110-420).

Competing interests

The authors declare no competing interests.

Author details

[1]Institute of Basic Medical Sciences, College of Medicine, National Cheng Kung University, Tainan, Taiwan
[2]Department of Physiology, College of Medicine, National Cheng Kung University, Tainan, Taiwan
[3]Institute of Clinical Medicine, College of Medicine, National Cheng Kung University, Tainan, Taiwan
[4]Department of Dermatology, Feinberg School of Medicine, Northwestern University, Chicago, IL, USA
[5]Department of Biochemistry and Molecular Genetics, University of Virginia School of Medicine, Charlottesville, VA 22908, USA
[6]Department of Pathology, National Cheng Kung University Hospital, College of Medicine, National Cheng Kung University, Tainan, Taiwan
[7]National Institute of Cancer Research, National Health Research Institutes, Tainan, Taiwan
[8]Department of Oncology, National Cheng Kung University Hospital, College of Medicine, National Cheng Kung University, Tainan, Taiwan
[9]Division of General Surgery, Department of Surgery, National Cheng Kung University Hospital, College of Medicine, National Cheng Kung University, Tainan, Taiwan
[10]Department of Biomedical Sciences, National Chung Cheng University, No.168, Sect. 1, University Rd., Minhsiung, Chiayi 621301, Taiwan
[11] Department of Internal Medicine, Kaohsiung Medical University Hospital, Kaohsiung, Taiwan
[12]Center for Cancer Research,, Kaohsiung Medical University, Kaohsiung, Taiwan

Received: 3 July 2024 / Accepted: 24 December 2024
Published online: 18 January 2025

References

1. Cerami E, et al. The cBio cancer genomics portal: an open platform for exploring multidimensional cancer genomics data. Cancer Discov. 2012;2(5):401–4.
2. Lohr M, et al. Frequency of K-ras mutations in pancreatic intraductal neoplasias associated with pancreatic ductal adenocarcinoma and chronic pancreatitis: a meta-analysis. Neoplasia. 2005;7(1):17–23.
3. Eser S, et al. Oncogenic KRAS signalling in pancreatic cancer. Br J Cancer. 2014;111(5):817–22.
4. Aguirre AJ, et al. Activated Kras and Ink4a/Arf deficiency cooperate to produce metastatic pancreatic ductal adenocarcinoma. Genes Dev. 2003;17(24):3112–26.
5. Hingorani SR, et al. Trp53R172H and KrasG12D cooperate to promote chromosomal instability and widely metastatic pancreatic ductal adenocarcinoma in mice. Cancer Cell. 2005;7(5):469–83.
6. Bryant KL, et al. Combination of ERK and autophagy inhibition as a treatment approach for pancreatic cancer. Nat Med. 2019;25(4):628–40.
7. Shibata H, et al. In vivo reprogramming drives Kras-induced cancer development. Nat Commun. 2018;9(1):2081–p.
8. Ren B, et al. Tumor microenvironment participates in metastasis of pancreatic cancer. Mol Cancer. 2018;17(1):108.
9. Carpenter ES, et al. Analysis of donor pancreata defines the transcriptomic signature and microenvironment of early pre-neoplastic pancreatic lesions. Cancer Discov. 2023;13(6):1324–45.
10. Lankadasari MB, et al. TAMing pancreatic cancer: combat with a double edged sword. Mol Cancer. 2019;18(1):48.
11. Lin Y, Xu J, Lan H. Tumor-associated macrophages in tumor metastasis: biological roles and clinical therapeutic applications. J Hematol Oncol. 2019;12(1):76.
12. Barnes TA, Amir E. HYPE or HOPE: the prognostic value of infiltrating immune cells in cancer. Br J Cancer. 2018;118(2):e5.
13. Cui R, et al. Targeting tumor-associated macrophages to combat pancreatic cancer. Oncotarget. 2016;7(31):50735–54.
14. Kemp SB, M. Pasca di Magliano, and, Crawford HC. *Myeloid Cell Mediated Immune Suppression in Pancreatic Cancer.* Cell Mol Gastroenterol Hepatol, 2021. 12(5): pp. 1531–1542.
15. Liou GY, et al. Mutant KRAS-induced expression of ICAM-1 in pancreatic acinar cells causes attraction of macrophages to expedite the formation of precancerous lesions. Cancer Discov. 2015;5(1):52–63.
16. Clark CE, et al. Dynamics of the immune reaction to pancreatic cancer from inception to invasion. Cancer Res. 2007;67(19):9518–27.
17. Zhu Y, et al. Tissue-Resident macrophages in Pancreatic Ductal Adenocarcinoma Originate from embryonic hematopoiesis and promote Tumor Progression. Immunity. 2017;47(2):323–e3386.
18. Carpenter ES, et al. KRT17high/CXCL8 + tumor cells display both classical and basal features and regulate myeloid infiltration in the pancreatic Cancer Microenvironment. Clin Cancer Res. 2024;30(11):2497–513.
19. Caronni N, et al. IL-1beta(+) macrophages fuel pathogenic inflammation in pancreatic cancer. Nature. 2023;623(7986):415–22.
20. Griesmann H et al. Pharmacological macrophage inhibition decreases metastasis formation in a genetic model of pancreatic cancer. Gut, 2016.
21. Wang CA, et al. DUSP2 regulates extracellular vesicle-VEGF-C secretion and pancreatic cancer early dissemination. J Extracell Vesicles. 2020;9(1):1746529.
22. Lin SC, et al. Suppression of dual-specificity phosphatase-2 by hypoxia increases chemoresistance and malignancy in human cancer cells. J Clin Invest. 2011;121(5):1905–16.
23. Hosein AN et al. Cellular heterogeneity during mouse pancreatic ductal adenocarcinoma progression at single-cell resolution. JCI Insight, 2019. 5(16).
24. Tsai WB, et al. Activation of Ras/PI3K/ERK pathway induces c-Myc stabilization to upregulate argininosuccinate synthetase, leading to arginine deiminase resistance in melanoma cells. Cancer Res. 2012;72(10):2622–33.
25. Klomp JE, et al. Determining the ERK-regulated phosphoproteome driving KRAS-mutant cancer. Science. 2024;384(6700):eadk0850.
26. Ye H, et al. Tumor-associated macrophages promote progression and the Warburg effect via CCL18/NF-kB/VCAM-1 pathway in pancreatic ductal adenocarcinoma. Cell Death Dis. 2018;9(5):453.
27. Fankhauser M et al. Tumor lymphangiogenesis promotes T cell infiltration and potentiates immunotherapy in melanoma. Sci Transl Med, 2017. 9(407).
28. Li WN, et al. Extracellular vesicle-associated VEGF-C promotes lymphangiogenesis and immune cells infiltration in endometriosis. Proc Natl Acad Sci U S A. 2020;117(41):25859–68.
29. Jung KK, et al. Identification of CD63 as a tissue inhibitor of metalloproteinase-1 interacting cell surface protein. EMBO J. 2006;25(17):3934–42.
30. Klomp JA, et al. Defining the KRAS- and ERK-dependent transcriptome in KRAS-mutant cancers. Science. 2024;384(6700):eadk0775.
31. Aran D, Hu Z, Butte AJ. xCell: digitally portraying the tissue cellular heterogeneity landscape. Genome Biol. 2017;18(1):220.
32. Guerra C, et al. Pancreatitis-induced inflammation contributes to pancreatic cancer by inhibiting oncogene-induced senescence. Cancer Cell. 2011;19(6):728–39.
33. Richards DM, Hettinger J, Feuerer M. Monocytes and macrophages in cancer: development and functions. Cancer Microenviron. 2013;6(2):179–91.
34. Chu X, Tian Y, Lv C. Decoding the spatiotemporal heterogeneity of tumor-associated macrophages. Mol Cancer. 2024;23(1):150.
35. Karayiannakis AJ, et al. Aberrant E-cadherin expression associated with loss of differentiation and advanced stage in human pancreatic cancer. Anticancer Res. 1998;18(6A):4177–80.
36. Hong SM, et al. Loss of E-cadherin expression and outcome among patients with resectable pancreatic adenocarcinomas. Mod Pathol. 2011;24(9):1237–47.
37. Dansranjavin T, et al. E-cadherin and DAP kinase in pancreatic adenocarcinoma and corresponding lymph node metastases. Oncol Rep. 2006;15(5):1125–31.
38. Ting DT, et al. Single-cell RNA sequencing identifies extracellular matrix gene expression by pancreatic circulating tumor cells. Cell Rep. 2014;8(6):1905–18.
39. Takahashi K, et al. Pancreatic tumor microenvironment confers highly malignant properties on pancreatic cancer cells. Oncogene. 2018;37(21):2757–72.
40. Tsai JH, Yang J. Epithelial-mesenchymal plasticity in carcinoma metastasis. Genes Dev. 2013;27(20):2192–206.
41. Venhuizen JH et al. P120 and E-cadherin: double-edged swords in tumor metastasis. Semin Cancer Biol, 2019.
42. Ichikawa K, et al. MCRIP1, an ERK substrate, mediates ERK-induced gene silencing during epithelial-mesenchymal transition by regulating the co-repressor CtBP. Mol Cell. 2015;58(1):35–46.
43. Tian Z, et al. TIMP1 derived from pancreatic cancer cells stimulates Schwann cells and promotes the occurrence of perineural invasion. Cancer Lett. 2022;546:215863.
44. Hermann CD et al. TIMP1 expression underlies sex disparity in liver metastasis and survival in pancreatic cancer. J Exp Med, 2021. 218(11).

Publisher's note